Originally presented as part of the ASPRS 2021 Annual Conference

UAV Remote Sensing Assessment of Crop Growth

Freda Elikem Dorbu, Leila Hashemi-Beni, Ali Karimoddini, and Abolghasem Shahbazi

Abstract

The introduction of unmanned-aerial-vehicle remote sensing for collecting high-spatial- and temporal-resolution imagery to derive crop-growth indicators and analyze and present timely results could potentially improve the management of agricultural businesses and enable farmers to apply appropriate solution, leading to a better food-security framework. This study aimed to analyze crop-growth indicators such as the normalized difference vegetation index (NDVI), crop height, and vegetated surface roughness to determine the growth of corn crops from planting to harvest. Digital elevation models and orthophotos generated from the data captured using multispectral, red/green/blue, and near-infrared sensors mounted on an unmanned aerial vehicle were processed and analyzed to calculate the various crop-growth indicators. The results suggest that remote sensing-based growth indicators can effectively determine crop growth over time, and that there are similarities and correlations between the indicators.

Introduction

During the last decade, there have been improvements in the agricultural sector through theoretical and technological developments in many fields, including chemistry, genetics, and robotics (Radoglou-Grammatikis *et al.* 2020), and there has been an increase in the estimated amount of investment toward the development of agricultural-based technology (Tsouros *et al.*, 2019). However, there is still a rising need to increase food production, because of the continuous increase in the human population and urbanization. The adoption of these scientific approaches aims to increase agricultural food by 70% by the year 2050, when the world's population is projected to be 9 billion (Grainger 2010; Perea-Moreno *et al.* 2019), with an increasing demand for crops from 2005 to 2050 (Tilman *et al.* 2011; Tian *et al.* 2021) and a stipulated decrease in cultivated area (Tsouros *et al.* 2019). Intensive use of available farmland to close the yield gaps and reduction of the expansion of agricultural lands could positively affect crop production and improve the supply chain necessary to meet crop demand (Foley *et al.* 2011; Tilman *et al.* 2011; J. Huang *et al.* 2019).

The linear relationship between population and agricultural growth necessitates the acceptance and advancement of a multi-disciplinary method that facilitates monitoring and evaluation of crop fields for growth assessment, through timely collection and analysis of farm data, to inform decision making (Popescu *et al.*, 2020). In addition, other outcomes from agricultural activities, such as the emission of 30% to 35% of greenhouse gases (Foley *et al.* 2011) and nitrogen pollution due to incomplete absorption by plants (Stuart *et al.* 2014), could be solved by the adoption of a well-structured interdisciplinary approach to optimizing production. Finally, agricultural stakeholders would not be burdened with the limitations of practicing traditional agronomy, which involves expensive and time-consuming methods (Wei *et al.* 2018).

Precision agriculture and smart farming technologies observe and measure an area to respond to spatial and temporal variability in crop fields (Jeppesen *et al.* 2018). This mechanism aims to maximize inputs for more rewarding output without disturbing natural resources, so as to advance environmental sustainability and quality (Mulla *et al.* 2002; Gołaś *et al.* 2020). Whipker and Akridge (2008) estimate that adoption of precision agriculture could contribute to an increase of more than 30% in US agribusiness. Precision and smart agriculture involve the use of sensors and software, coupled with other technologies, to collect and transfer data without the assistance of humans. Precision farming enables monitoring of crop growth and other agronomy processes such as fertilizer application, disease detection, and irrigation routines. The use of such technologies helps in obtaining timely data from the farmland for crop management and decision making in an efficient manner (Aubert *et al.* 2012; Mulla 2013). However, prevailing issues such as compatibility, complexity, and interoperability slow down the rate at which precision agriculture is adopted (Aubert *et al.* 2012). Shadrin *et al.* (2020) provide an overview of the issues and challenges associated with precision agriculture. The main objectives in adopting precision agriculture are to increase crop yield, improve product quality, ensure efficient usage of production inputs, save energy, and prevent environmental pollution (Radoglou-Grammatikis *et al.* 2020).

Remote sensing has been an important technology in precision agriculture (Shafiee *et al.* 2021). In agriculture it involves the use of platforms such as unmanned aerial vehicles (UAVs), satellites, and piloted aircraft to observe and measure reflected radiation from the surfaces of soil and plant materials to ascertain their features. The technology has been applied to different agricultural applications (Pinter *et al.* 2003; Hashemi-Beni and Gebrehiwot 2020; Weiss *et al.* 2020), such as determining crop yield and biomass (Shanahan *et al.* 2001; Chao *et al.* 2019), water stress and nutrients (Tilling *et al.* 2007; Ihuoma and Madramootoo 2017), and weed infestations (Thorp and Tian 2004; Y. Huang *et al.* 2018), as well as detecting plant diseases (Buja *et al.* 2021). Most remote sensing-based agriculture studies have been based on images acquired by either satellite or piloted vehicle to monitor vegetation levels (Mora *et al.* 2017). However, satellite imagery has low spatial resolution, and limitations on the acquisition of temporal-resolution imagery because of the potential unavailability of the satellite at the stipulated time. In addition, image collection by

Freda Elikem Dorbu is with the Computational Data Science and Engineering Department, North Carolina A&T State University, Greensboro, NC 27411 (fedorbu@aggies.ncat.edu).

Leila Hashemi-Beni is with the Geomatics Program, Built Environment Department, North Carolina A&T State University, Greensboro, NC 27411 (lhashemibeni@ncat.edu).

Ali Karimoddini is with the Electrical Engineering Department, North Carolina A&T State University, Greensboro, NC 27411 (akarimod@ncat.edu).

Abolghasem Shahbazi is with the Agricultural Science Department, North Carolina A&T State University, Greensboro, NC 27411 (ash@ncat.edu).

Contributed by Alper Yilmaz, August 30, 2021 (sent for review August 30, 2021).

Photogrammetric Engineering & Remote Sensing
Vol. 87, No. 12, December 2021, pp. 891–899.
0099-1112/21/891–899

doi: 10.14358/PERS.21-00060R2

satellites is sometimes disrupted by environmental conditions. The use of piloted aircraft is also costly, and deploying multiple flights to acquire extra crop images is often challenging. UAV-based remote sensing systems for crop monitoring are fairly cost-effective, easily retrieve field data, and are very fast. UAVs can be flown on demand at varying altitudes to capture high-spatial- and temporal-resolution data over a crop field. These attributes have contributed to the advancement of precision agriculture. UAVs can be equipped with sensors to monitor crops, evaluate the field, and provide information to assist in identifying problems such as diseases and pests and guide farmers to quickly solving farm-related issues.

UAVs have been used in precision agriculture for several applications, such as weed mapping, monitoring and estimation of vegetation yield, irrigation management, crop spraying, and monitoring of vegetation health and detection of diseases (Tsouros *et al.* 2019; Hashemi-Beni and Gebrehiwot 2020). Allred *et al.* (2018) investigated the use of UAVs in identifying drainage pipes on farms, which are useful to farmers for controlling the amount of water on a field. A lidar sensor mounted on a UAV can assist in determining crop production and health status; images retrieved by lidar have been used for textural analysis to estimate total plant volume and soil surface for particular crops (Christiansen *et al.* 2017). UAVs have been also used in collecting thermal and multispectral information from a field to estimate water stress and the health status of pomegranate crops in Greece (Katsigiannis *et al.* 2016). The nitrogen status of rice has been determined by analyzing hyperspectral data captured using a UAV (Zheng *et al.* 2016). The use of time-series vegetation indices can identify varying crop classes and also indicate growth patterns in crops (de Souza *et al.* 2015). Prediction of wheat yield has been achieved using multi-sensor and multi-temporal remote sensing images taken on different dates (Wang *et al.* 2014). X. Zhou *et al.* (2017) used both UAV-generated single and multi-temporal vegetation indices to predict rice yield. Shafiee *et al.* (2021) have shown that multi-temporal indices generated from time-series data are more highly correlated with crop yield than are single vegetation indices. Time-series UAV data have also been used to determine the pattern of height and phenological changes in each growth cycle of corn of different genotypes (Han *et al.* 2019). Yeom *et al.* (2019) used time-series vegetation indices to determine the differences between no-tillage and conventional-tillage agricultural practices and their effects.

In spite of these works, more research is still required to evaluate the performance of UAV time-series data for precision agriculture. In that context, our research aimed to investigate UAV-based time-series vegetation indices for monitoring and determining the impact of fertilizer application and prescribed burns at the beginning of planting on phenological changes in crops over time. In addition, we conduct analyses of time-series UAV data for monitoring and evaluation of the crop condition in a controlled cornfield, determine the efficiency of remote sensing-based crop-growth indicators and the similarities among them, and estimate the biomass yield of the crop in the field using the time-series UAV data.

The article is organized as follows: The next section explains the study area and data collected for the research. Then the research materials and methodology are described, followed by a presentation and discussion of the results. Last come conclusions and a summary of future research.

Study Area and Data

The study area is a 2-acre controlled test plot, of size 415×210 ft, located at the North Carolina A&T State University research farm in Greensboro, North Carolina. As shown in Figure 1, the plot was divided into three different blocks to evaluate the performance of UAV time-series data for crop-growth assessment considering the effects of burning (killing the winter crop with herbicide) and/or fertilizing before planting. Blocks 1 and 2 (each 415×70 ft) both had winter crops that were not burned before the new planting. The difference between them is that block 1 received fertilizer and block 2 did not. Block 3 (450×120 ft) received a traditional treatment: burning the winter crop with herbicide before the new planting, and applying the recommended amounts of NPK fertilizer. Corn was planted on the entire field on 24 April 2020.

Figure 1. Study area: the block design of the field. Block 1 was not burned but fertilizer was applied; block 2 was not burned and received no fertilizer; and block 3 was both burned and fertilized.

A UAV was used for collection of red/green/blue and near-infrared imagery over the controlled plot; eight ground control points were implemented for georeferencing. The UAV collected time-series data at 40 and 70 m every 2 wk from seeding time (April 2020) to harvesting (August 2020). The flight altitude of 40 m provided higher-resolution imagery while reducing the image's coverage area, thus increasing the flight duration and number of images required to cover the area of interest. Both flights for each collection took place on the same day, with one flight deployed at the end of the other. This approach aimed to compare maps generated from the images of the field and study the impact of the imagery resolution on the crop-growth assessment. Table 1 describes the time-series data collected.

Table 1. Data collected by two sensors mounted on a UAV at different flight altitudes.

Number of GCPs	Sensors	Flight Altitudes	Spatial Resolutions	Temporal Resolution
8	RGB, NIR	40 and 70 m	1 and 1.9 cm	2 weeks apart

GCP = ground control point; NIR = near-infrared; RGB = red/green/blue; UAV = unmanned aerial vehicle.

Methodology

Data Processing

A structure-from-motion approach was used for 3D reconstruction of the farmland from the 80% overlapping images collected by the UAV. These methods use feature-based image-matching methods and collinearity conditions from camera alignment for, respectively, image-to-image registration and 3D surface construction (Hashemi-Beni *et al.*, 2018). The ground control points were used for georeferencing to ensure the accuracy of the reconstructed 3D images. A digital elevation model (DEM) map was created after georeferencing, which was used for orthorectification and creation of the 3D model.

Identification of Crop-Growth Indicators

Crop-growth indicators are used as indices to determine changes that occur on a field during the growing season. Determination of these indicators enables timely collection of data from the field for making decisions and taking prompt action if required. The three important indicators of growth change studied in the research are the normalized difference vegetation index, roughness length, and crop-height change from the time of planting to harvesting.

Normalized Difference Vegetation Index (NDVI)

The NDVI, an extensively used vegetation index, indicates the greenness or the photosynthetic status of a vegetative area. It assists in determining the locations of water, bare soil, and plants, as well as whether plants are healthy or stressed. This knowledge is based on the reflectance received from crops. Crops that are healthy and actively photosynthesizing absorb most of the red light they receive and reflect much of the near-infrared light, and the estimated amount of red light reflected by stressed vegetation is greater than near-infrared. NDVI is calculated as (Hashim *et al.* 2019)

$$\mathrm{NDVI} = \frac{(\mathrm{NIR} - \mathrm{Red})}{(\mathrm{NIR} + \mathrm{Red})} \tag{1}$$

Values range from −1 to +1 (Meneses-Tovar 2011; Alface *et al.* 2019), with those between −1 and 0 indicating bare soil, roads, dead plants, or water and those between 0 and 1 indicating live plants (Table 2). In positive values, lower ones indicate stressed or unhealthy plants, and higher ones indicate healthy plants. In this research, time-series NDVI raster layers were obtained by using a raster map algebra using Equation 1.

Vegetated-Surface Roughness Length

Roughness length (RL) is an expression of the variability of elevation of a topographic surface at a given scale, where the scale of analysis is determined by the size of the landforms or geomorphic features of interest, either local or regional. It shows the heterogeneity in land surface. Roughness of vegetated surfaces is dependent on the mean canopy height, the canopy structure, and the plant density (Jasinski and Crago 1999; Urrego *et al.* 2021). Although roughness length is identified by several models as a function of structural parameters of vegetation such as canopy area index, frontal area index (Raupach 1994; Hu *et al.* 2020), and leaf area index (Myneni *et al.* 2002; Hu *et al.* 2020), it closely correlates with NDVI during the period of crop growth (M. Yu *et al.* 2017; Schaudt and Dickinson 2000).

Surface RL measurements depict the nature of features of the land or farm. Table 3 describes the surface of a field based on estimated RL values obtained from analysis. A very rough field has vegetation like a young dense forest, indicating the springing up of new vegetation with 70% canopy density.

For this study, RL was estimated by first computing the total curvature of the individual digital elevation models and then deriving a focal statistic for calculating the standard deviation within a moving neighborhood window of 3×3 pixels. The raster was log-transformed to normalize and reduce skewness. The roughness index is calculated as (Korzeniowska *et al.* 2018)

$$\mu = \log_{10} \sqrt{\frac{\sum_{i=1}^{n} \left(x_i - \bar{x}_i\right)^2}{n}} \tag{2}$$

where x_i represents the curvature value of the center cell, $\bar{x}_i$ represents the mean curvature, and n is the number of pixels (for a 3×3 kernel).

Table 2. Normalized difference vegetation index (NDVI) values indicating vegetation classes (Hashim *et al.* 2019).

Vegetation Class	Description	NDVI Value
Non-vegetation	Barren areas, built-up areas, road network	−1 to 0.199
Low vegetation	Shrub and grassland	0.2 to 0.5
High vegetation	Temperate and tropical urban forest	0.501 to 1.0

Table 3. Roughness-length thresholds (Wieringa 1992; J. Yu *et al.* 2021).

Roughness Length	Landscape Features	Class
0.03	Flat terrain with very low vegetation or grass	Open
0.10	Cultivated area, low crops	Roughly open
0.25	Open landscape, scattered shelter belts	Rough
0.5	Young dense forest	Very rough
1.0	Mature forest	Closed
≥2.0	Irregular distribution of large forest with clearings	Chaotic

Plant Height

Plant height, which is the distance from the highest point of a plant to the lowest point (ground), assists in evaluating both plant growth and yield (Bendig *et al.* 2015). It provides relevant parameters for assessing plant physiology, genetic traits, and environmental impacts (Malambo *et al.* 2018). Figure 2 shows the stages of growth of maize from planting time to harvest time, indicating the stipulated height at each time period and the percentages of water and fertilizer required (Colless 1992). The percentages were determined in the laboratory and will be used for comparison and validation of the UAV-generated information.

In this research, a time-series DEM was processed and used for estimating changes in crop heights across growth stages. The DEM of each time stamp was subtracted from the DEM of the beginning time, 30 April (planting stage). The resultant raster presents the height change, enabling identification of the growth cycle of the crop, which in turn assists in choosing appropriate crop-management practices from the available husbandry options. Height change can be represented mathematically as

$$\text{Height change} = ((\text{Current\_time[DEM]} - \text{Planting\_time[DEM]})) \tag{3}$$

Statistical Analysis

A quantitative analysis was conducted to study the time-series assessment of the growth indices from planting to harvesting. Thirty-six checkpoints with random distribution were generated for each treatment block on the field (Figure 3). Changes in NDVI, RL, and crop height over time were analyzed for the checkpoints.

Results

Analysis of the time-series UAV and geospatial data was done in Agisoft Photoscan and ArcGIS. All UAV images, taken at both 40 and 70 m, were processed, but for demonstration purposes, only the results from 70 m are shown. Time-series digital elevation models were used in estimating crop height and vegetated RL change, whereas orthomosaics were used in assessing time-series NDVI.

Crop-Growth Indicators

This section provides the results of the three indicators used to determine maize growth from the time of planting to harvest.

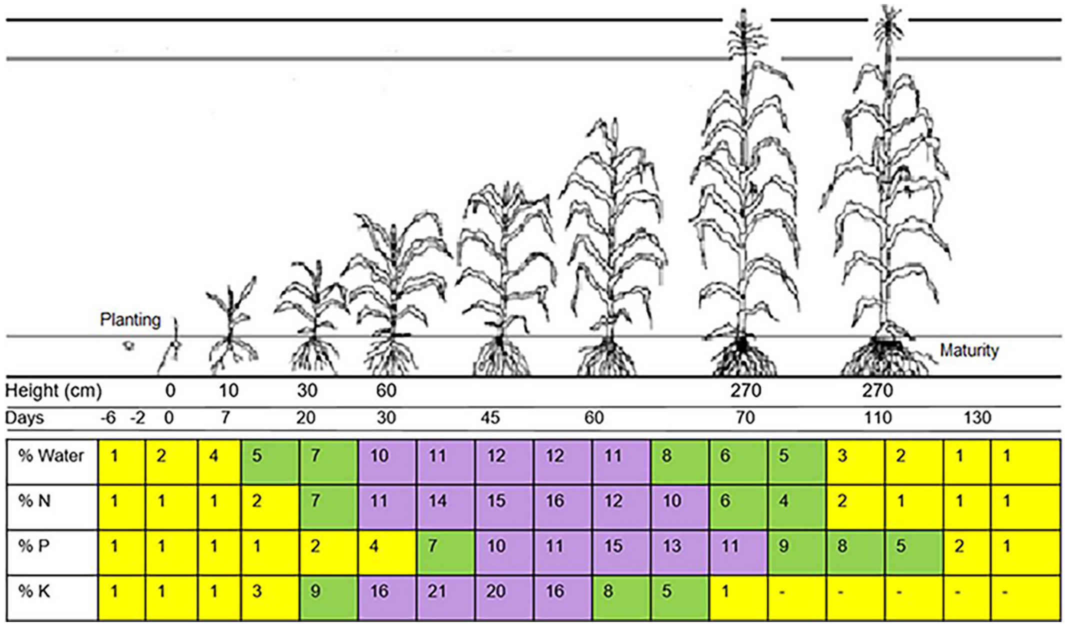

Figure 2. Maize growth cycle (Colless 1992), based on the application of recommended water and fertilizer (N, P, K), coupled with the presence of other essential elements such as sunlight.

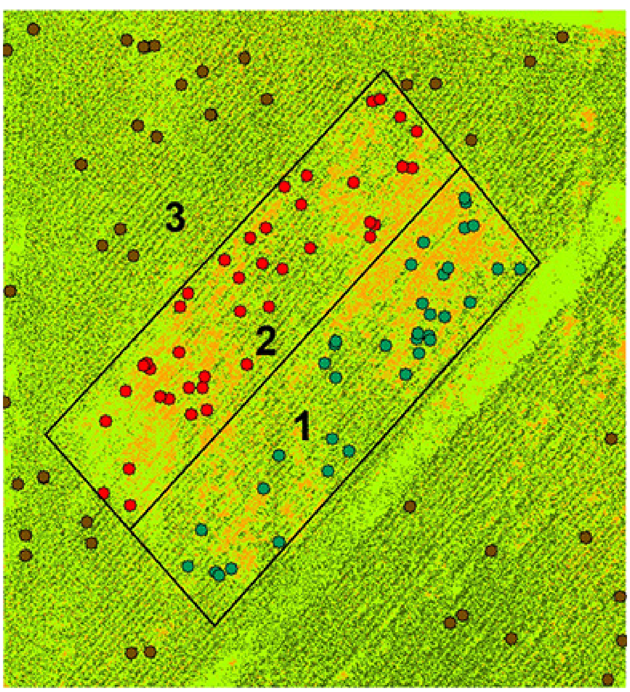

Figure 3. Checkpoints with random distribution in the treatment blocks. These checkpoints were used for assessing and comparing the crop-growth indicators (NDVI, RL, and height change) in the three blocks.

Time-Series NDVI

Results from NDVI analysis affirm the various block treatments applied to the study area. The variation in crop biomass yield across different blocks is due to the differences in block treatments. The time-series NDVI from April through August (Figure 4) shows the progression on the field from nearly bare earth to vast biomass development.

NDVI estimation for the first two blocks is high on 30 April due to the presence of winter crops on the field before and after the sowing of maize seeds. There was a concurrent increase in biomass in the whole field, including high vegetation looking like a mature forest (NDVI 0.5–1) in the first two blocks from 12 to 29 May. However, biomass in these blocks began to deplete from 29 May until 26 June, when the depletion was massive. This was caused by the gradual withering of the winter crops and weeds in the region due to high temperatures in the summer.

There was a gradual increase in NDVI for block 3 from 30 April through 12 June, when there was a decline in biomass (Figure 5). This was due to the high average temperature of 84°F, which led to high evapotranspiration from the leaves and the soil surface in the field without replacement of water through irrigation, leading to the death of winter crops and thus low vegetation presence. Temperature and precipitation (Figure 6) are climatic conditions which greatly affect vegetation growth (Buitenwerf *et al.* 2015). Changes in climate cause variability in vegetation growth and influence functions that are associated with vegetation (Li *et al.* 2019). An example is the occurrence of frost, which leads to a reduction in vegetation biomass on a maize field (Raun *et al.* 2005). There was not much change in biomass on our whole field from 27 July to 11 August, as corn is ready for harvest as silage and not much phenological development occurred.

Time-Series RL

The vegetated-surface RL variation in the study area depicted a heterogeneous field along several rows. This heterogeneity implies a crop at different growth stages, and inconsistency in cultivation practices. The RL of the field on 30 April indicates open or flat terrain with both low vegetation or low grass-like biomass and vegetation looking like scattered shelter belts. The field can be classified as a rough open space. Vegetation increased by 12 May, when the field looked like a dense forest (Figure 7).

A marginal shift from heterogeneous to homogenous over the period 26 May to 12 June is associated with the increase in biomass along specific rows. From 26 June to 11 August, the study area excluding the alleyway was more closed, consisting of a lot of vegetation in the form of mature forest with a few chaotic instances. Except for blocks 1 and 2, in which some parts were indicated as rough, and the alleyway, the field was almost homogenous (Figure 8f). Corn crops at this time are usually ready to be harvested, since there is not

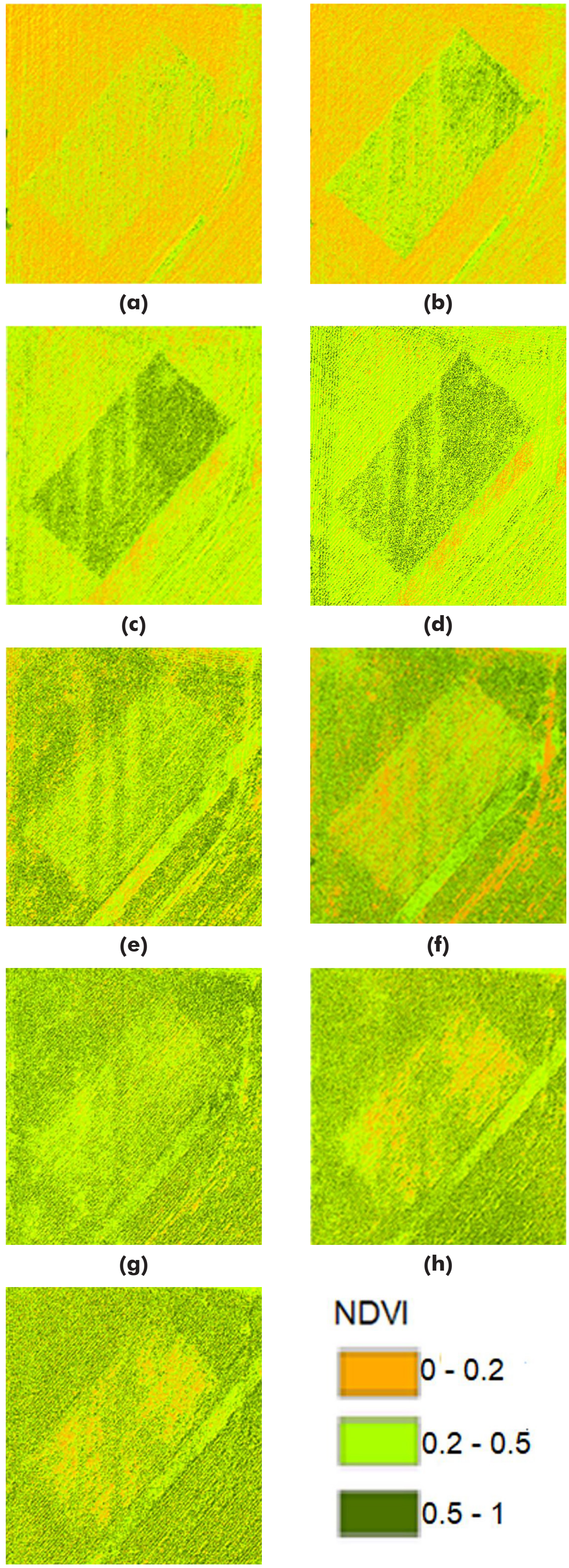

Figure 4. Time-series normalized difference vegetation index generated from unmanned-aerial-vehicle data on (a) 30 April 30, (b) 12 May, (c) 26 May, (d) 29 May, (e) 12 June, (f) 26 June, (g) 9 July, (h) 27 July, and (i) 11 August.

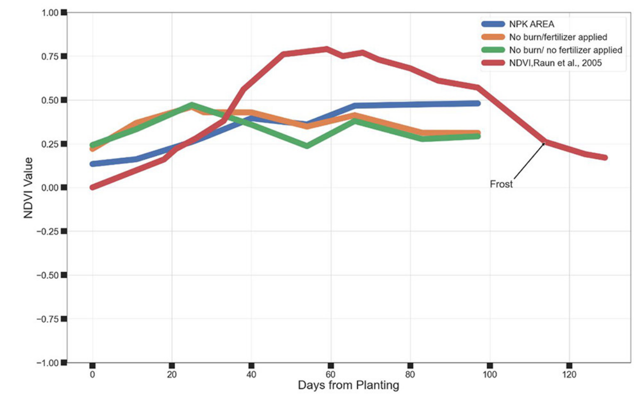

Figure 5. Time-series normalized difference vegetation index (NDVI) values for the three block treatments in our study area, compared to the study by Raun *et al.* (2005).

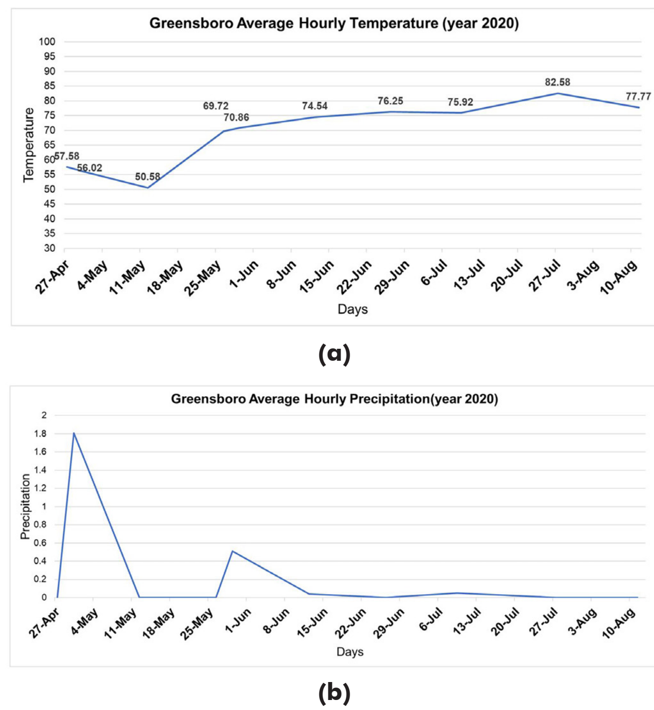

Figure 6. Weather conditions in the study area: (a) average hourly temperature and (b) average hourly precipitation.

much more change in the growth of the crop, and there is uniformity in the growth cycle with less alteration.

Time-Series Crop Height

Figure 9 presents the UAV-based time-series crop-height changes. Although the height estimation did not differentiate the types of vegetation present in the controlled field, the variation in height at the various growth stages assisted in differentiating corn from the winter crops. The decline in crop height on 12 June in the first two blocks was because the average hourly temperature was 75°F, with low precipitation (Figure 6), which led to the death of weeds and winter crops that could not survive the hot summer weather. However, there was an increase in crop height in block 3 due to the absence of winter crops and competition from weeds. The decline in crop height for all three blocks on 9 July shows the effect of lagging climatic conditions leading to the lodging of plants.

Lodging is a result of strong winds and rainstorms (Acorsi *et al.* 2019). These weather conditions lead to corn plants leaning flat to the ground (L. Zhou *et al.* 2020), and sometimes roots becoming dislocated from the soil or stems breaking,

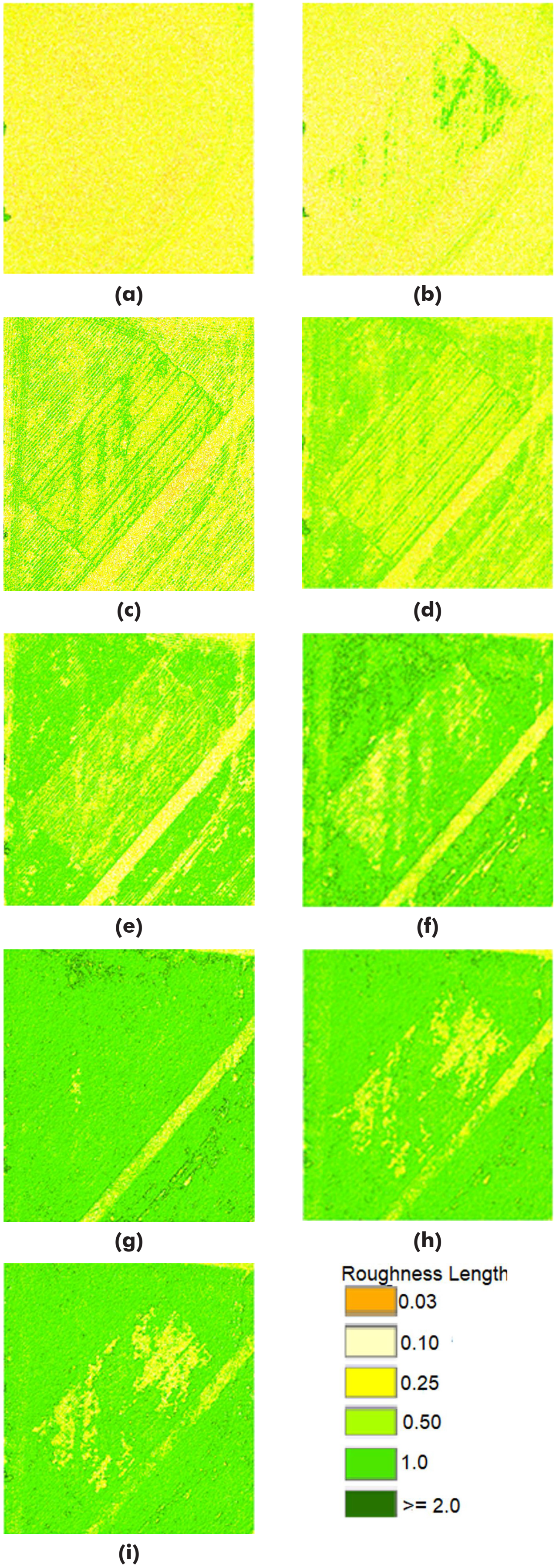

Figure 7. Time-series roughness length, showing the variability of the field surface based on the growth of crops and the canopy density on (a) 30 April, (b) 12 May, (c) 26 May, (d) 29 May, (e) 12 June, (f) 26 June, (g) 9 July, (h) 27 July, and (i) 11 August.

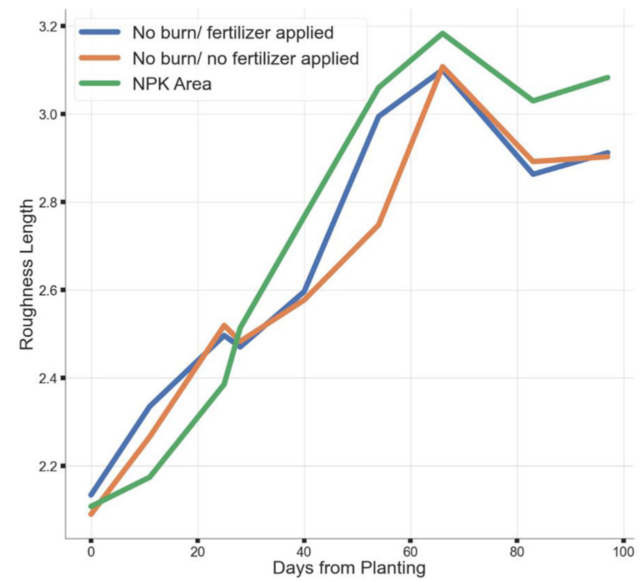

Figure 8. Time-series averaged roughness length for the three treatment blocks from planting to maturity.

reducing maize height. On 9 July, the average hourly precipitation in the study area was 0.05 in, with a wind speed of 13 mi per hr from the north-northeast. Corn height decreased after 9 July in all blocks and then resumed normal growth after 27 July (Figure 10). A correlation matrix for crop height in the three treatment blocks (Figure 11) showed a correlation of 0.93 between blocks 1 and 3, implying a 93% similarity in corn-height changes in the two blocks, which could be due to the presence of fertilization in both. The change in crop height in block 3 (treated with NPK fertilizer) was within a range of 0.5 to 1.5 m on 11 August, whereas the other blocks recorded changes of 0.1 to 0.5 m. Crop heights in the first two blocks are lower because of the competition for nutrients and moisture from unburned weeds.

The UAV DEM generated from this study for each time stamp was used to estimate the surface roughness of the field and the change in crop height. Crops that are unevenly spaced and have a lot of seeds per hole encourage competition among the crop and weeds, leading to variability in the canopy surface and to crop failure. The use of UAV multi-temporal data captured the variability caused by these parameters, which can assist in replanting of crops to improve growth and eventually increase crop yield. Changes in crop height are attributed to phenological development in the crop. It is necessary to calculate the height to ensure that the crop has attained acceptable growth before harvesting and to determine fertilizer and water application during the growth cycle. The differences in biomass yield over the entire period assist in detecting unhealthy crops and informing decisions as to intervention to rescue the crop. They also assist in predicting crop yield based on reflection from time-series data of phenotypic development.

Conclusion

UAV has proven to be a reliable source for the collection of multi-temporal data irrespective of time sensitivity of the growth season. It is easily accessible and very flexible, and images can be taken repeatedly. Placement of ground control points on the field of study validates the UAV images collected and ensures accuracy of the 3D image constructed through georeferencing of point clouds. The UAV vegetation indices

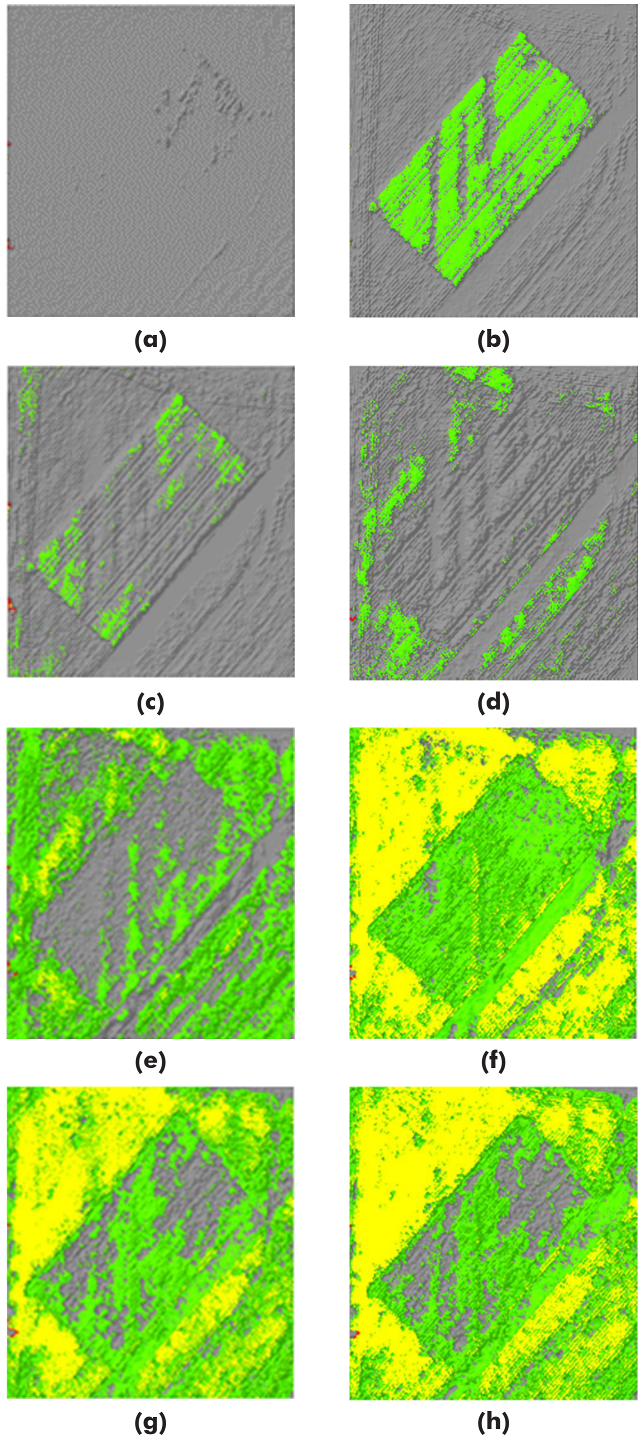

Figure 9. Time-series crop height from planting to harvest using unmanned-aerial-vehicle data on (a) 12 May, (b) 26 May, (c) 29 May, (d) 12 June, (e) 26 June, (f) 9 July, (g) 27 July, and (h) 11 August.

evaluated in this study quickly indicated a change in vegetation from the time of planting to the time of harvest, compared to the traditional method of monitoring a field, which is time-consuming and labor-intensive. The normalized

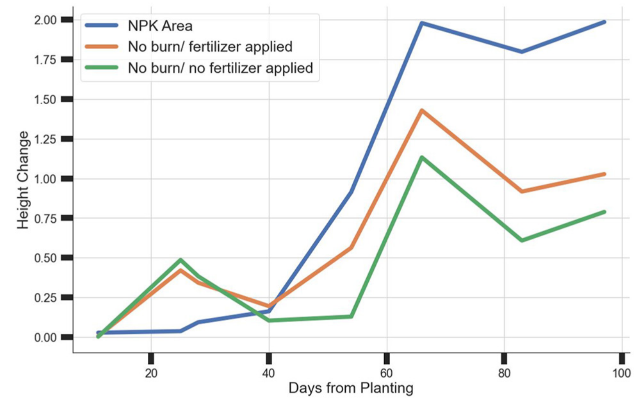

Figure 10. Averaged time-series crop-height changes the three treatment blocks from planting to maturity.

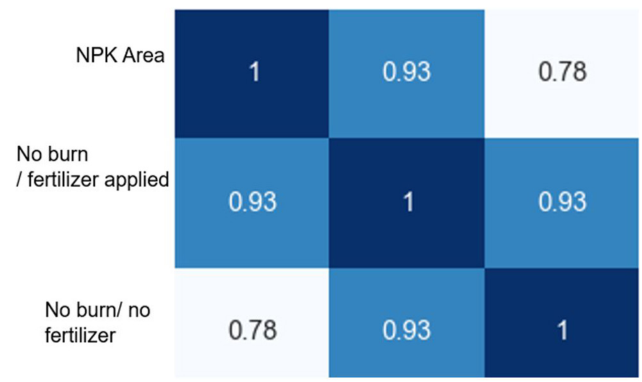

Figure 11. Correlation matrix for crop height in the three treatment blocks.

difference vegetation index provided clear information on the vegetation status of the corn crop. Images acquired by remote sensing were used to determine the health status of the crop through estimating the NDVI. Low NDVI values imply crops that are either unhealthy or moderately healthy, whereas high values close to 1 indicate a healthy crop and provide information on biomass yield. UAV-generated time-series results indicated both healthy and unhealthy crop, with high and low vegetation in the field. This analytical result from the NDVI correlates with the vegetated-surface roughness length for each period, which indicates that the level of vegetation can be determined by other indices, not only NDVI. Remote sensing detected the presence of more biomass in the control block compared to the other two blocks, and the RL values implied that the field was heterogeneous due to factors such as plant spacing and density, plant height, and canopy structure for most of the growth cycle. Remote sensing technology indicated that the study area was a heterogeneous field for most of the period of crop growth, becoming slightly homogeneous in the latter stage of the cycle. The height-change results assisted in identifying the impact of weather conditions on the maize crop. In the future, we will use deep learning for classification purposes and time-series analysis.

Acknowledgments

This work was supported in part by the National Science Foundation under grants 1832110 (Developing a Robust, Distributed, and Automated Sensing and Control System for Smart Agriculture) and 1800768 (Remote Sensing for Flood Modeling and Management).

References

Acorsi, M. G., M. Martello and G. Angnes. 2019. Identification of maize lodging: A case study using a remotely piloted aircraft system. Engenharia Agrícola 39 (special issue):66–73.

Alface, A. B., S. B. Pereira, R. Filgueiras and F. F. Cunha. 2019. Sugarcane spatial-temporal monitoring and crop coefficient estimation through NDVI. *Revista Brasileira de Engenharia Agrícola e Ambiental* 23(5):330–335.

Allred, B., N. Eash, R. Freeland, L. Martinez and D. Wishart. 2018. Effective and efficient agricultural drainage pipe mapping with UAS thermal infrared imagery: A case study. *Agricultural Water Management* 197:132–137.

Aubert, B. A., A. Schroeder and J. Grimaudo. 2012. IT as enabler of sustainable farming: An empirical analysis of farmers' adoption decision of precision agriculture technology. *Decision Support Systems* 54(1):510–520.

Bendig, J., K. Yu, H. Aasen, A. Bolten, S. Bennertz, J. Broscheit, M. L. Gnyp and G. Bareth. 2015. Combining UAV-based plant height from crop surface models, visible, and near infrared vegetation indices for biomass monitoring in barley. *International Journal of Applied Earth Observation and Geoinformation* 39:79–87.

Buitenwerf, R., L. Rose and S. I. Higgins. 2015. Three decades of multi-dimensional change in global leaf phenology. *Nature Climate Change* 5(4):364–368. https://doi.org/10.1038/nclimate2533.

Buja, I., E. Sabella, A. G. Monteduro, M. S. Chiriacò, L. De Bellis, A. Luvisi and G. Maruccio. 2021. Advances in plant disease detection and monitoring: From traditional assays to in-field diagnostics. *Sensors* 21(6):2129.

Chao, Z., N. Liu, P. Zhang, T. Ying and K. Song. 2019. Estimation methods developing with remote sensing information for energy crop biomass: A comparative review. *Biomass and Bioenergy* 122:414–425.

Christiansen, M. P., M. S. Laursen, R. N. Jørgensen, S. Skovsen and R. Gislum. 2017. Designing and testing a UAV mapping system for agricultural field surveying. *Sensors* 17(12):2703.

Colless, J. (1992). Maize growing. NSW Agriculture: Orange, Australia.

de Souza, C.H.W., E. Mercante, J. A. Johann, R.A.C. Lamparelli and M. A. Uribe-Opazo. 2015. Mapping and discrimination of soya bean and corn crops using spectro-temporal profiles of vegetation indices. *International Journal of Remote Sensing* 36(7):1809–1824.

Foley, J. A., N. Ramankutty, K. A. Brauman, E. S. Cassidy, J. S. Gerber, M. Johnston, N. D. Mueller, C. O'Connell, D. K. Ray, P. C. West, C. Balzer, E. M. Bennett, S. R. Carpenter, J. Hill, C. Monfreda, S. Polasky, J. Rockström, J. Sheehan, S. Siebert, D. Tilman and D.P.M. Zaks. 2011. Solutions for a cultivated planet. *Nature* 478(7369):337–342.

Goła′, M., P. Sulewski, A. W′s, A. Kłoczko-Gajewska and K. Pogodzi′ska. 2020. On the way to sustainable agriculture—eco-efficiency of Polish commercial farms. *Agriculture* 10(10):438.

Grainger, M. 2010. World Summit on Food Security (UN FAO, Rome, 16–18 November 2009). *Development in Practice* 20(6):740–742.

Han, L., G. Yang, H. Dai, H. Yang, B. Xu, H. Feng, Z. Li and X. Yang. 2019. Fuzzy clustering of maize plant-height patterns using time series of UAV remote-sensing images and variety traits. *Frontiers in Plant Science* 10:926. https://doi.org/10.3389/fpls.2019.00926.

Hashemi-Beni, L. and A. Gebrehiwot. 2020. Deep learning for remote sensing image classification for agriculture applications. *The International Archives of the Photogrammetry, Remote Sensing and Spatial Information Sciences* 44:51–54.

Hashemi-Beni, L., J. Jones, G. Thompson, C. Johnson and A. Gebrehiwot. 2018. Challenges and opportunities for UAV-based digital elevation model generation for flood-risk management: A case of Princeville, North Carolina. *Sensors* 18(11):3843.

Hashim, H., Z. Abd Latif and N. A. Adnan. 2019. Urban vegetation classification with NDVI threshold value method with very high resolution (VHR) Pleiades imagery. *The International Archives of the Photogrammetry, Remote Sensing and Spatial Information Sciences* 42(4/W16):237–240.

Hu, X., L. Shi, L. Lin and V. Magliulo. 2020. Improving surface roughness lengths estimation using machine learning algorithms. *Agricultural and Forest Meteorology* 287:107956. https://doi.org/10.1016/j.agrformet.2020.107956.

Huang, J., H. Ma, F. Sedano, P. Lewis, S. Liang, Q. Wu, W. Su, X. Zhang and D. Zhu. 2019. Evaluation of regional estimates of winter wheat yield by assimilating three remotely sensed reflectance datasets into the coupled WOFOST–PROSAIL model. *European Journal of Agronomy* 102:1–13.

Huang, Y., K. N. Reddy, R. S. Fletcher and D. Pennington. 2018. UAV low-altitude remote sensing for precision weed management. *Weed Technology* 32(1):2–6.

Ihuoma, S. O. and C. A. Madramootoo. 2017. Recent advances in crop water stress detection. *Computers and Electronics in Agriculture* 141:267–275.

Jasinski, M. F. and R. D. Crago. 1999. Estimation of vegetation aerodynamic roughness of natural regions using frontal area density determined from satellite imagery. *Agricultural and Forest Meteorology* 94(1):65–77. https://doi.org/10.1016/S0168-1923(98)00129-4.

Jeppesen, J. H., E. Ebeid, R. H. Jacobsen and T. S. Toftegaard. 2018. Open geospatial infrastructure for data management and analytics in interdisciplinary research. *Computers and Electronics in Agriculture* 145:130–141.

Katsigiannis, P., L. Misopolinos, V. Liakopoulos, T. K. Alexandridis and G. Zalidis. 2016. An autonomous multi-sensor UAV system for reduced-input precision agriculture applications. Pages PP–PP in *2016 24th Mediterranean Conference on Control and Automation (MED)*, held in Athens, Greece, 21–24 June 2016. Edited by J. Editor. Location: IEEE.

Korzeniowska, K., N. Pfeifer and S. Landtwing. 2018. Mapping gullies, dunes, lava fields, and landslides via surface roughness. *Geomorphology* 301:53–67.

Li, W., J. Du, S. Li, X. Zhou, Z. Duan, R. Li, S. Wu, S. Wang and M. Li. 2019. The variation of vegetation productivity and its relationship to temperature and precipitation based on the GLASS-LAI of different African ecosystems from 1982 to 2013. *International Journal of Biometeorology* 63(7):847–860. https://doi.org/10.1007/s00484-019-01698-x.

Malambo, L., S. C. Popescu, S. C. Murray, E. Putman, N. A. Pugh, D. W. Horne, G. Richardson, R. Sheridan, W. L. Rooney, R. Avant, M. Vidrine, B. McCutchen, D. Baltensperger and M. Bishop. 2018. Multitemporal field-based plant height estimation using 3D point clouds generated from small unmanned aerial systems high-resolution imagery. *International Journal of Applied Earth Observation and Geoinformation* 64:31–42.

Meneses-Tovar, C. L. 2011. NDVI as indicator of degradation. *Unasylva* 62(238):39–46.

Mora, A., T.M.A. Santos, S. Łukasik, J.M.N. Silva, A. J. Falcão, J. M. Fonseca and R. A. Ribeiro. 2017. Land cover classification from multispectral data using computational intelligence tools: A comparative study. *Information* 8(4):147.

Mulla, D. J., P. Gowda, W. C. Koskinen, B. R. Khakural, G. Johnson and P. C. Robert. 2002. Modeling the effect of precision agriculture: Pesticide losses to surface waters. In *Terrestrial Field Dissipation Studies*, ACS Symposium Series vol. 842, edited by E. L. Arthur, A. C. Barefoot and V. E. Clay, 304–317. Location: American Chemical Society.

Mulla, D. J. 2013. Twenty five years of remote sensing in precision agriculture: Key advances and remaining knowledge gaps. *Biosystems Engineering* 114(4):358–371.

Myneni, R. B., S. Hoffman, Y. Knyazikhin, J. L. Privette, J. Glassy, Y. Tian, Y. Wang, X. Song, Y. Zhang, G. R. Smith, A. Lotsch, M. Friedl, J. T. Morisette, P. Votava, R. R. Nemani and S. W. Running. 2002. Global products of vegetation leaf area and fraction absorbed PAR from year one of MODIS data. *Remote Sensing of Environment* 83(1–2):214–231. https://doi.org/10.1016/S0034-4257(02)00074-3.

Perea-Moreno, M.-A., E. Samerón-Manzano and A.-J. Perea-Moreno. 2019. Biomass as renewable energy: Worldwide research trends. *Sustainability* 11(3):863.

Pinter Jr, P. J., J. L. Hatfield, J. S. Schepers, E. M. Barnes, M. S. Moran, C.S.T. Daughtry and D. R. Upchurch. 2003. Remote sensing for crop management. *Photogrammetric Engineering and Remote Sensing* 69(6):647–664.

Popescu, D., F. Stoican, G. Stamatescu, L. Ichim and C. Dragana. 2020. Advanced UAV–WSN system for intelligent monitoring in precision agriculture. *Sensors* 20(3):817.

Radoglou-Grammatikis, P., P. Sarigiannidis, T. Lagkas and I. Moscholios. 2020. A compilation of UAV applications for precision agriculture. *Computer Networks* 172:107148. https://doi.org/10.1016/j.comnet.2020.107148.

Raun, W., J. B. Solie, K. L. Martin, K. W. Freeman, M. L. Stone, G. V. Johnson and R. W. Mullen. 2005. Growth stage, development, and spatial variability in corn evaluated using optical sensor readings. *Journal of Plant Nutrition* 28(1):173–182.

Raupach, M. R. 1994. Simplified expressions for vegetation roughness length and zero-plane displacement as functions of canopy height and area index. *Boundary-Layer Meteorology* 71(1):211–216. https://doi.org/10.1007/BF00709229.

Schaudt, K. J. and R. E. Dickinson. 2000. An approach to deriving roughness length and zero-plane displacement height from satellite data, prototyped with BOREAS data. *Agricultural and Forest Meteorology* 104(2):143–155.

Shadrin, D., A. Menshchikov, A. Somov, G. Bornemann, J. Hauslage and M. Fedorov. 2020. Enabling precision agriculture through embedded sensing with artificial intelligence. *IEEE Transactions on Instrumentation and Measurement* 69(7):4103–4113. https://doi.org/10.1109/TIM.2019.2947125.

Shafiee, S., L. M. Lied, I. Burud, J. A. Dieseth, M. Alsheikh and M. Lillemo. 2021. Sequential forward selection and support vector regression in comparison to LASSO regression for spring wheat yield prediction based on UAV imagery. *Computers and Electronics in Agriculture* 183:106036.

Shanahan, J. F., J. S. Schepers, D. D. Francis, G. E. Varvel, W. W. Wilhelm, J. M. Tringe, M. R. Schlemmer and D. J. Major. 2001. Use of remote′sensing imagery to estimate corn grain yield. *Agronomy Journal* 93(3):583–589.

Stuart, D., R. L. Schewe and M. McDermott. 2014. Reducing nitrogen fertilizer application as a climate change mitigation strategy: Understanding farmer decision-making and potential barriers to change in the US. *Land Use Policy* 36:210–218.

Thorp, K. R. and L. F. Tian. 2004. A review on remote sensing of weeds in agriculture. *Precision Agriculture* 5(5):477–508.

Tian, X., B. A. Engel, H. Qian, E. Hua, S. Sun and Y. Wang. 2021. Will reaching the maximum achievable yield potential meet future global food demand? *Journal of Cleaner Production* 294:126285. https://doi.org/10.1016/j.jclepro.2021.126285.

Tilling, A. K., G. J. O'Leary, J. G. Ferwerda, S. D. Jones, G. J. Fitzgerald, D. Rodriguez and R. Belford. 2007. Remote sensing of nitrogen and water stress in wheat. *Field Crops Research* 104(1–3):77–85.

Tilman, D., C. Balzer, J. Hill and B. L. Befort. 2011. Global food demand and the sustainable intensification of agriculture. *Proceedings of the National Academy of Sciences, USA* 108(50):20260–20264.

Tsouros, D. C., S. Bibi and P. G. Sarigiannidis. 2019. A review on UAV-based applications for precision agriculture. *Information* 10(11):349.

Urrego, J.P.F., B. Huang, J. S. Næss, X. Hu and F. Cherubini. 2021. Meta-analysis of leaf area index, canopy height and root depth of three bioenergy crops and their effects on land surface modeling. *Agricultural and Forest Meteorology* 306:108444. https://doi.org/10.1016/j.agrformet.2021.108444.

Wang, L., Y. Tian, X. Yao, Y. Zhu and W. Cao. 2014. Predicting grain yield and protein content in wheat by fusing multi-sensor and multi-temporal remote-sensing images. *Field Crops Research* 164:178–188.

Wei, M., B. Qiao, J. Zhao and X. Zuo. 2018. Application of remote sensing technology in crop estimation. Pages PP–PP in *2018 IEEE 4th International Conference on Big Data Security on Cloud (BigDataSecurity), IEEE International Conference on High Performance and Smart Computing (HPSC), and IEEE International Conference on Intelligent Data and Security (IDS)*, held in Omaha, Neb., 3–5 May 2018. Edited by J. Editor. Location: IEEE.

Weiss, M., F. Jacob and G. Duveiller. 2020. Remote sensing for agricultural applications: A meta-review. *Remote Sensing of Environment* 236:111402. https://doi.org/10.1016/j.rse.2019.111402.

Whipker, L. D. and J. T. Akridge. 2008. *2008 Precision Agricultural Services Dealership Survey Results*. Retrieved from

Wieringa, J. 1992. Updating the Davenport roughness classification. *Journal of Wind Engineering and Industrial Aerodynamics* 41(1–3):357–368. https://doi.org/10.1016/0167-6105(92)90434-C.

Yeom, J., J. Jung, A. Chang, A. Ashapure, M. Maeda, A. Maeda and J. Landivar. 2019. Comparison of vegetation indices derived from UAV data for differentiation of tillage effects in agriculture. *Remote Sensing* 11(13):1548.

Yu, J., T. Stathopoulos and M. Li. 2021. Estimating exposure roughness based on Google Earth. *Journal of Structural Engineering* 147(3):04020353.

Yu, M., B. Wu, N. Yan, Q. Xing and W. Zhu. 2017. A method for estimating the aerodynamic roughness length with NDVI and BRDF signatures using multi-temporal Proba-V data. *Remote Sensing* 9(1):6.

Zheng, H., X. Zhou, T. Cheng, X. Yao, Y. Tian, W. Cao and Y. Zhu. 2016. Evaluation of a UAV-based hyperspectral frame camera for monitoring the leaf nitrogen concentration in rice. In *2016 IEEE International Geoscience and Remote Sensing Symposium (IGARSS)*, held in Beijing, China, 10–15 July 2016.

Zhou, L., X. Gu, S. Cheng, G. Yang, M. Shu and Q. Sun. 2020. Analysis of plant height changes of lodged maize using UAV-LiDAR data. *Agriculture* 10(5):146.

Zhou, X., H. B. Zheng, X. Q. Xu, J. Y. He, X. K. Ge, X. Yao, T. Cheng, Y. Zhu, W. X. Cao and Y. C. Tian. 2017. Predicting grain yield in rice using multi-temporal vegetation indices from UAV-based multispectral and digital imagery. *ISPRS Journal of Photogrammetry and Remote Sensing* 130:246–255.